Materials Today Bio 33 (2025) 102074

Contents lists available at ScienceDirect

Materials Today Bio

journal homepage: www.journals.elsevier.com/materials-today-bio

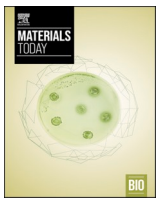

Hyaluronic acid-anchored nanoparticles co-delivering emodin and siRNA confers protection against rheumatoid arthritis via macrophage polarization

Muting Qin [a,1], Penglu Chen [a,1], Huanxue Chen [a,1], Feng Liu [b], Wei He [c,**], Enyang Yao [d,*]

[a] Department of Rheumatology and Immunology, Shengjing Hospital of China Medical University, Shenyang, Liaoning, 110004, China
[b] Transportation Research Institute (IMOB), Hasselt University, Martelare Nlaan, 42-3500, Hasselt, Belgium
[c] Department of Thoracic Surgery, The Shengjing Hospital of China Medical University, Shenyang, Liaoning, 110004, China
[d] Department of Orthopedics, The Shengjing Hospital of China Medical University, Shenyang, Liaoning, 110004, China

ARTICLE INFO

Keywords:
Rheumatoid arthritis
Macrophage polarization
Fe-based metal-organic framework
Emodin
KEAP1
Co-delivery nanosystem

ABSTRACT

Macrophages are key effector cells in the pathogenesis of rheumatoid arthritis (RA), and the pro-inflammatory M1 phenotype accelerates the release of cytokines and exacerbates joint inflammation. In this study, a modified Fe-based metal-organic framework (Fe-MOF) was designed for RA treatment by co-delivering emodin (EM) and small interfering RNA of Kelch-like ECH-associated protein 1 (siKEAP1). To target inflammatory lesions, hyaluronic acid (HA) was encapsulated on the surface of nanoparticles, thereby specifically binding to CD44 receptor overexpressed on M1 macrophage membranes. From the characterization, the synthesized EM/siKEAP1@Fe-MOF@HA exhibited a stable physicochemical profile and pH-responsive property. As expected, EM/siKEAP1@Fe-MOF@HA could effectively target macrophages and promote internalization through clathrin-mediated endocytosis. Both *in vitro* and *in vivo* experiments confirmed that the internalized nanoparticles reduced the levels of inflammatory factors and reactive oxygen species and promoted M2 macrophage polarization by releasing EM and downregulating KEAP1. EM/siKEAP1@Fe-MOF@HA can also alleviate the pathological features of RA mice. More importantly, EM/siKEAP1@Fe-MOF@HA maintained an optimistic biosafety profile, avoiding liver and kidney toxicity and damage to major organs. Overall, this nano-delivery system reduced the pathological and inflammatory responses of RA by targeting macrophages and mediating their polarization, and thus could serve as a safe and effective strategy in the treatment of RA.

1. Introduction

Rheumatoid arthritis (RA) is an autoimmune disease of uncertain etiology characterized by chronic joint inflammation and cartilage damage, which may involve systemic organs and cause progressive disability [1,2]. The global prevalence of RA is approximately 1 %, with affected patients exhibiting a two-fold increased risk of malignancy and cardiovascular disease development compared to healthy controls [3,4]. In the pathogenesis of RA, macrophages are key effector cells that are heavily enriched in synovium to produce pro-inflammatory cytokines [5]. During this process, macrophage polarization is blocked, leading to the predominance of the pro-inflammatory M1 phenotype, which may further exacerbate the joint inflammation [6,7]. Therefore, maintaining M1/M2 macrophage balance as well as immune homeostasis are important strategies to ameliorate inflammation in RA.

Although the development of the pharmaceutical industry has provided more options for the treatment of RA, the long-term safety of commonly used medications to maintain joint function, as well as non-steroidal anti-inflammatory drugs and glucocorticoids in the management of RA remains controversial [8,9]. Therefore, the exploration for effective and low-toxicity drugs is urgently needed. Emodin (EM) is an anthraquinone derivative found in a variety of natural herbs [10,11].

* Corresponding author. Department of Orthopedics, The Shengjing Hospital of China Medical University, Sanhao Street 36, Heping District, Shenyang, Liaoning, 110004, China.
** Corresponding author. Department of Thoracic Surgery, The Shengjing Hospital of China Medical University, Sanhao Street 36, Heping District, Shenyang, Liaoning, 110004, China.
E-mail addresses: 13889858921@163.com (W. He), yaoenyang@163.com (E. Yao).
[1] Muting Qin, Penglu Chen and Huanxue Chen are co-first authors and contributed equally to this work.

https://doi.org/10.1016/j.mtbio.2025.102074
Received 8 May 2025; Received in revised form 30 June 2025; Accepted 8 July 2025
Available online 10 July 2025

This active ingredient has pharmacological significance and exerts antioxidant and anti-inflammatory effects [12]. EM has been found to alleviate RA by reducing the immune infiltration and the release of pro-inflammatory cytokines [13]. Systemic introduction of EM also synergistically modulates multiple cytokines, thereby inhibiting immune cell infiltration in RA and promoting the repair of joint function [14]. In addition to natural active compound, the introduction of gene drugs is also of great significance in improving the therapeutic strategies of RA. A previous study has shown that Kelch-like ECH-associated protein 1 (KEAP1) is highly expressed in RA fibroblast-like synoviocytes [15]. The overexpression of KEAP1 in RA was also accompanied by the increased levels of oxidative stress [16]. Thus, small interfering (siRNA) of KEAP1 (siKEAP1) may possess therapeutic potential for RA, but how to co-deliver EM and siRNA to maintain the stability of their physicochemical properties and improve their bioavailability has become an urgent issue.

With the advantages of abundant voids, large specific surface area, and stable structure, metal-organic framework (MOF) nanomaterials are widely used in drug delivery systems [17,18]. However, the toxicity of metal ions and organic ligands has raised concerns, thus prompting the production of Fe-based MOF (Fe-MOF) [19]. Fe-MOF has received special attentions due to its low toxicity and good biocompatibility, and has expanded the biomedical applications of conventional MOFs [20,21]. Hyaluronic acid (HA) can specifically target various receptors that are overexpressed on the cell membrane of M1-polarized macrophages, which provides a feasible solution for the inability of nanoparticles to target lesions [22]. As a natural linear polysaccharide, HA is not only non-toxic and biodegradable, but also has anti-inflammatory and antioxidant bioactivities that can be used for RA therapy [23,24].

Based on the above theoretical background, our team designed the Fe-MOF-based nanoparticles that can co-deliver EM and siKEAP1 while anchoring HA for its purpose of targeting macrophages. Theoretically, the nanosystem can ensure biosafety, target macrophages, and inhibit the inflammatory response in RA by promoting the macrophage polarization towards M2 phenotype (Fig. 1). To confirm the above conjecture, the nanomaterials were characterized in this study and their anti-RA potential was confirmed by *in vitro* and *in vivo* experiments. We expect that this drug delivery system will provide a safer and more effective strategy for the treatment of RA.

2. Methods

2.1. Chemicals and materials

The Fe-MOF (MIL-100), HA, and EM were purchased from Sigma (catalog number: LEYH9ACF8736; purity: 98 %), Xi'an Ruixi Biological Technology (catalog number: R-Y065), and Macklin Biochemical Technology Co., Ltd. (catalog number: E808871; purity: 98 %), respectively. Lipopolysaccharide (LPS, L8880), agarose (A8190), Triton X-100 (T8200), fetal bovine serum (FBS, S9030), trypsin (T1300), and DCFH-DA (D6470) were supplied by Beijing Solarbio Science & Technology Co.,Ltd. Fluorescein isothiocyanate (FITC, ST2065), Tris-HCl (pH6.8, ST768; pH8.8, ST789), nucleic acid dye ethidium bromide (EB, D0128), polyformaldehyde (P0099), 4′,6-diamidino-2-phenylindole (DAPI, C1005), and antifade mounting medium (p0126) were purchased from Shanghai Beyotime Biotechnology. Chlorpromazine (CPZ, HY-12708), Nystatin (HY-17409), incomplete Freund's adjuvant (HY-153808A), and Colchicine (HY-16569) were obtained from MedChemExpress LLC. Primary antibodies of glyceraldehyde-3-phosphate dehydrogenase (GAPDH, ab181602) and KEAP1 (ab227828), as well as second antibodies (IgG H&L [HRP], ab6721; IgG H&L [Alexa Fluor® 647], ab150079; IgG H&L [Alexa Fluor® 488], ab150077) were purchased from Abcam. Besides, anti-iNOS (22226-1-AP) and anti-CD206 (18704-1-AP) antibodies were obtained from Proteintech Group, Inc. The anti-Nrf2 antibody (AF5298) was obtained from the Affinity Biosciences. The sequences of siKEAP1 were designed in the Designer of Small Interfering RNA website as following: SS Sequence GGUCAAGUACGACUGCGAACA; and AS Sequence UUCGCAGUCGUACUUGACCCA.

2.2. Synthesis of nanoparticles

Fe-MOF@HA: The Fe-MOF material was prepared into a homogeneous suspension with a final concentration of 2 mg/mL by ultrasonic treatment, mixed with HA (2 mg/mL) for 30 min under ultrasound, and washed with deionized water for three times to obtain Fe-MOF@HA.

EM@Fe-MOF: Fe-MOF was dispersed in ethanol solution by sonication, followed by the addition of 1.5 mg EM dissolving in ethanol. The solution was stirred at 200 rpm for 24 h, and then centrifuged at 8000 rpm for 5 min. The final product EM@Fe-MOF was obtained by washing

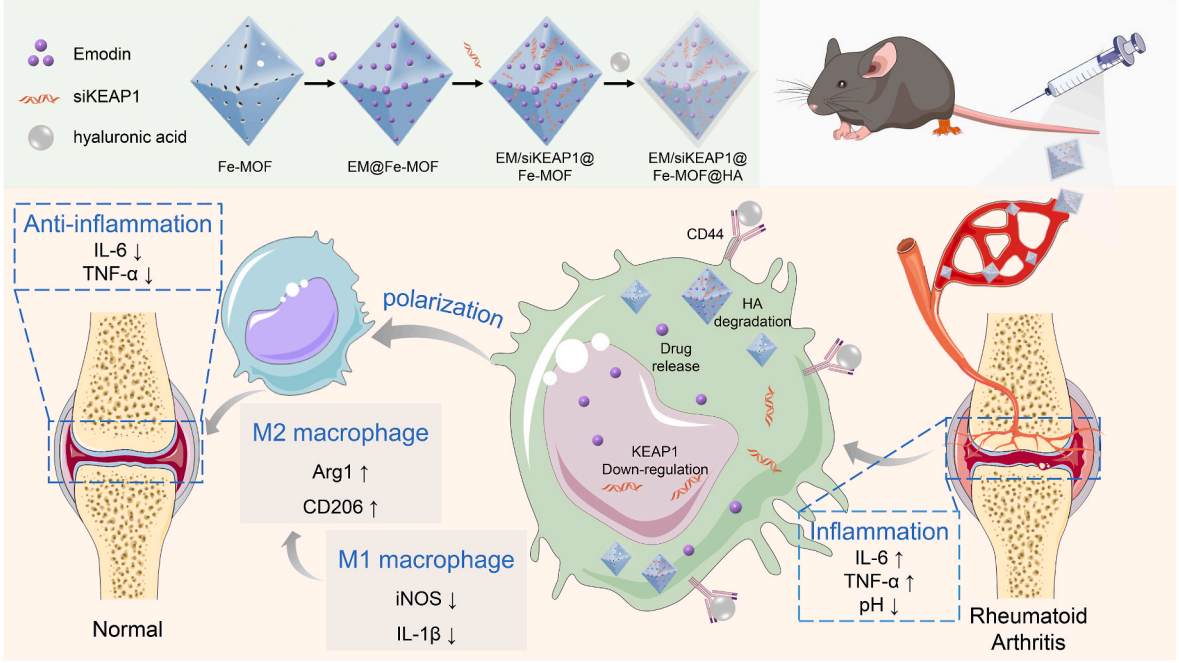

Fig. 1. Schematic illustration of EM/siKEAP1@Fe-MOF@HA synthesis and its *in vivo* application for RA therapy.

several times with ethanol to remove the excess EM. The eluate was also collected to calculate the loading efficiency of EM.

EM/siKEAP1@Fe-MOF: The synthesized EM@Fe-MOF was incubated with siKEAP1 at various N/P ratios (0:1, 1:1, 5:1, 10:1, 15:1, 20:1) and stirred for 12 h to facilitate adsorption. The resulting mixture was then centrifuged at 10,000 rpm for 10 min, followed by three washes to obtain the EM/siKEAP1@Fe-MOF complexes. The eluate was also collected to evaluate the loading efficiency of siRNA.

EM/siKEAP1@Fe-MOF@HA: 4 mg of HA was dissolved in 2 mL of ultrapure water and added dropwise to the EM/siKEAP1@Fe-MOF solution under continuous stirring for 30 min. The obtained solution was filtered (0.22 μm) and lyophilized to yield the EM/siKEAP1@Fe-MOF@HA nanocomposites, which was stored for further use.

2.3. Physicochemical properties evaluation of nanoparticles

To characterize nanomaterials, Fourier transform infrared spectroscopy (FTIR, TENSOR-37, Bruker) was used to detect the molecular structure. For this, lyophilized powder of samples from Fe-MOF, EM, EM@Fe-MOF, and EM@Fe-MOF@HA groups was weighed with 2 mg each. After compression, the characteristic peaks of each group were detected using FTIR. The micromorphology and particle size of these samples were determined by transmission electron microscopy (TEM, HT-7700, Hitachi) and laser particle size analyzer (Nano ZS90, Malvern), respectively. Leveraging the nitrogen adsorption property of the nanocomplexes, the Brunauer-Emmett-Teller (BET) method was employed to detect the specific surface area and pore diameter of Fe-MOF, Fe-MOF@HA, and EM/siKEAP1@Fe-MOF@HA. These samples were also assayed for zeta potential using zeta potentiometer (Nano ZS90, Malvern). To evaluate the stability of EM/siKEAP1@Fe-MOF@HA, its lyophilized powder was placed in the phosphate buffered saline (PBS) or 10 % FBS, and the nanoparticles were assayed for their particle size and polydispersity index (PDI) every 12 h of consecutive 144 h.

2.4. Loading efficiency of EM and siRNA

To examine the loading efficiency of EM and siKEAP1, we initially prepared their respective standard working solutions and established calibration curves for quantitative analysis. Then, the eluent from the preparation process was collected to detect for its absorption value at 330 nm. The free content of EM and siRNA was calculated according to the standard curve and the loading efficiency was calculated according to the following equation: Loading Efficiency (%) = $(W_{initial}\text{-}W_{free})/W_{final}$, where $W_{initial}$ represents the total amount of EM/siKEAP1 initially added, W_{free} indicates the free EM/siKEAP1 in the supernatant, and W_{final} denotes the mass of final obtained EM/siKEAP1@Fe-MOF@HA nanoparticles.

2.5. Agarose gel electrophoresis

The 1 g of agarose was placed into a conical flask, where 50 mL of 1 × TBE buffer was subsequently added. The conical flask was then heated until the agarose was completely dissolved, followed by the addition of 2 μL of EB. Behind this step, the agarose was cooled and solidified in the mold and placed in the electrophoresis tank. After loading the samples, electrophoresis was performed at 120V. Finally, the gel was photographed under UV light to observe the migration blocking of siRNAs at different N/P ratios.

2.6. In vitro release of EM and siKEAP1

The EM/siKEAP1@Fe-MOF@HA nanoparticles were dispersed in dialysis bags (intercepted molecular weight: 2 kDa) containing 2 mL PBS under different pH (5.4 or 7.4). The sealed dialysis bags were immersed in the bottle containing PBS (20 mL) at 37 °C in the dark. At certain time intervals (0, 8, 12, 24, 36, 48 h), samples were removed to measure the absorbance of the supernatant. The rate of drug release was calculated according to the concentration of drug in PBS/initial concentration of drug loaded in nanoparticles.

Prior to detecting the release of siKEAP1, standard solutions of siKEAP1 were prepared (6.25, 12.5, 25, 50, and 100 nM). Afterwards, EM/siKEAP1@Fe-MOF@HA with a final concentration of 100 nM siKEAP1 was loaded into a dialysis bag and dispersed in 5 mL of PBS at 100 rpm at 37 °C. At 0, 8, 12, 24, 36, and 48 h, 1 mL of dialysate was collected to determine the concentration of siKEAP1 and replenished with an equal amount of fresh PBS. Finally, the release rate of siKEAP1 was calculated based on the manner described above.

2.7. Cell culture

Macrophages RAW264.7 (mouse, CL-0190) and THP-1 (human, CL-0233) were purchased from Wuhan Pricella Biotechnology Co., Ltd. and maintained in RPMI-1640 medium (C11875500BT, Gibco) containing Penicillin-Streptomycin (SV30010, Hyclone) and FBS under conventional conditions. After adhesion, cells were successively stimulated with LPS (10 μg/mL) for 48 h to induce activation and then treated with FITC-labelled nanomaterials with a concentration of 10 μg/mL.

2.8. Quantitative real-time polymerase chain reaction (qPCR)

Cells and tissues were lysed with Trizol (15596018, Invitrogen) to release total RNAs, followed by a reverse transcription reaction to synthesize cDNA. After mixing cDNA templates and primers, the samples were subjected to PCR amplification on a Bio-rad instrument (CFX96Touch) for PCR reaction. The reaction conditions were set as follows: 40 cycles consisting of 95 °C for 3 min, 95 °C for 12 s, and 62 °C for 40 s. Detailed primer sequences are shown in Table 1. The mRNA expression of the target gene relative to GAPDH was calculated using the $2^{-\Delta\Delta CT}$ method.

2.9. Cellular uptake

Logarithmically growing cells were inoculated into a six-well plate at a density of 5×10^5/well, activated by LPS, and then treated with FITC-labelled nanomaterials at a concentration of 10 μg/mL for 2 h. The medium containing nanomaterials was removed and washed thrice with PBS. After digestion with trypsin, the cells were resuspended in PBS and analyzed for the fluorescence intensity using a flow cytometer (CytoFLEX S, Beckman).

The cells were inoculated and activated using the same method, followed by the addition of 10 μg/mL of FITC-labelled EM/siKEAP1@Fe-MOF@HA for continuous culture of 2, 4, 8, and 12 h to observe the time-dependence of cellular uptake. At the end of the incubation, the drug-containing medium was removed and washed thrice with PBS. Subsequently, the cells were fixed and stained by DAPI for 10 min. After sealing with antifade mounting medium, the uptake of fluorescence was observed using a confocal laser scanning microscope (CLSM, TCS SP8, Leica).

To further determine the detailed uptake mechanism, the same method was adopted to activate cells for 48 h. Subsequently, the cells were treated with CPZ (10 μg/mL), Nystatin (15 μg/mL), and Colchicine (5 μg/mL), respectively, for 1 h. After the treatment with FITC-labelled EM/siKEAP1@Fe-MOF@HA at a concentration of 10 μg/mL for 4 h, the fluorescence intensity of each group was analyzed by the flow cytometry.

2.10. Cell counting-8 (CCK-8)

Cell suspensions were inoculated in 96-well plates until complete adherence. Afterwards, cells were treated with (10 μg/mL) for 48 h, followed by the co-culture with different concentrations of EM/

Table 1
Sequences of primers used in qPCR.

Gene	Forward primer sequence (5′–3′)	Reverse primer sequence (5′–3′)
TNF-α (human)	CACGCTCTTETGGCTGCT	GCTFCFCACTCGGGGTTC
IL-1β (human)	CCAGCTACGAATCTCCGACC	TATCCTGTCCCTGGAGGTGG
IL-6 (human)	ACCCCCAGGAGAAGATTCCA	CAGCTCTGGCTTGTTCCTCA
Arg-1 (human)	CGCCAAGTCCAGAACCATAG	TCCCCATAATCCTTCACATCAC
KEAP1 (human)	GTGGAGACAGAGACCTGGACTTT	TGTCAACCCGGTCACTTCACTCA
GAPDH (human)	GAAGGTCGGAGTCAACGGAT	CTTCCCGTTCTCAGCCATGT
TNF-α (mouse)	CAGGCGGTGCCTATGTCTC	CGATCACCCCGAAGTTCAGTTCAGTAG
IL-1β (mouse)	TGTGACGTTCCC ATTAGACAG	TGTGACGTTCCCATTAGACAG
IL-6 (mouse)	AGTTCCTCTCTGCAAGAGACTTC	CTGCAACTGCATCATCCTTCT
Arg-1 (mouse)	TGTCCCTATGACAGCTCCTT	GCATCCACCCAATGACACAT
KEAP1 (mouse)	AGCGTGGAGAGATATGAGCC	ATCATCCCCCACTCATTCCT
GAPDH (mouse)	TGTGGGCATCAATGGATTTGG	ACACCATGTATTCCGGGTCAAT

qPCR, quantitative real-time polymerase chain reaction.

siKEAP1@Fe-MOF@HA (0, 2.5, 5, 10, 20, 40, 80 μg/mL) for one day. Following the standard procedure of the CCK-8 kit (C0037, Beyotime), 10 μL of CCK-8 reaction solution was added to each well. After incubation for 2 h, the absorbance of each well at 450 nm was measured by a microplate reader (DR-3518G, Wuxi Hiwell Diatek).

2.11. Immunofluorescence

The activated cells were treated with each group of nanomaterials (10 μg/mL) for 24 h. Then, cells were clambered, immobilized, and perforated with 1 % Triton-X 100 for 5–10 min. After washing with PBS, an appropriate amount of blocking solution was added to each sample for 30 min's incubation at room temperature. Following this, diluted anti-iNOS (1:150) and anti-CD206 (1:200) antibodies were added for incubation overnight. The next day, samples were maintained with diluted mixture of IgG H&L and DAPI at 1:500 for 30–60 min away from light. After washing and sealing, the samples were scanned and photographed by a CLSM (TCS SP8, Leica). For ROS detection, cells were mixed with DCFH-DA (diluted at 1:1000) to fluorescently label ROS and then incubated in the dark for 30 min. After removing the unincorporated dye, the cells were observed under a CLSM, followed by the quantification of fluorescence intensity using ImageJ.

For ankle tissues, we followed conventional methods for the preparation of tissue slices, including fixation, dehydration, transparency, wax dipping, embedding, and sectioning. After dewaxing and hydrating, slices were heated for antigen repair. Method of antibody incubation and result records are the same as described above.

2.12. Detection of NO

To investigate the changes in the pro-inflammatory capacity of macrophages, we sonicated the cells (300 w for 3 s, interval 7 s for 3 min) in accordance with the kit instructions (ml076493, Mlbio). The ratio of the number of cells (10,000) to the volume of extraction solution (mL) was maintained between 500:1 and 1000:1. After centrifugation at 10000*g*, 4 °C for 15 min, the absorbance of each sample was examined at 550 nm.

2.13. Enzyme linked immunosorbent assay (ELISA)

The levels of IL-6 and TNF-α in the samples were evaluated by ELISA assay kits (human IL-6: ml028583, Mlbio; human TNF-α: ml064303, Mlbio; mouse IL-6: ml063159, Mlbio; mouse TNF-α: ml002095, Mlbio). Briefly, 50 μL of samples were added to the plate, followed by the addition of 50 μL of the working solution. After incubation at 37 °C for 30 min, cells were washed repeatedly for 4 times. Then, 50 μL of Colorant A and 50 μL of Colorant B were added to each well for the reaction of 15 min. Finally, the reaction was terminated by adding 50 μL of termination solution. Finally, the absorbance value of each well was measured at 450 nm.

2.14. Western blotting

Total proteins in cells and tissues were extracted by lysate for quantification. Subsequently, proteins were separated by sodium dodecyl sulfate polyacrylamide gel electrophoresis. The proteins were then transferred to a polyvinylidene fluoride membrane for the incubation with anti-KEAP1 (1:2000), anti-Nrf2 (1:500) and anti-GAPDH (1:10,000) antibodies overnight. On the second day, the membrane was cleaned and incubated with the secondary antibody working solution for 60 min. Finally, the film was developed with enhanced chemiluminescence (P1000, ApplyGen), scanned, and archived. The gray values of protein bands were captured using ImageJ, while the relative protein expression of KEAP1 or Nrf2 was calculated using GAPDH as an internal reference.

2.15. Animals

Thirty 8-week-old male DBA/1J mice weighting at 18–20 g were procured from the Experimental Animal Center of Yangzhou University for the construction of a collagen-induced RA model. For the first immunization, mice were injected subcutaneously with an emulsion of 100 μg of bovine type II collagen (20022, Chondrex) and complete Freund's adjuvant. To enhance immunization, mice were then injected 3 weeks later with an emulsion of equal amounts of bovine type II collagen and incomplete Freund's adjuvant. Another week later, the successful construction of the model was confirmed. Then, the mice in the treatment group were administered EM@Fe-MOF@HA, siKEAP1@Fe-MOF@HA, and EM/siKEAP1@Fe-MOF@HA (1.5 mg/kg) via tail vein injection, respectively. The control and model groups received an equivalent volume of normal saline. The treatment was processed once every 3 days for a total of 5 times. After each treatment, the body weight, paw thickness, and clinical score of arthritic inflammation of mice were recorded. The clinical scoring criteria for the degree of arthritis inflammation were 0: normal; 1: mild redness and swelling of ankle and wrist joints; 2: moderate redness and swelling of ankle or wrist joints; 3: severe redness and swelling of the paws, including the fingertips; 4: severe inflammation of the limbs including multiple joints. The final score of each mouse, ranging from 0 to 16, was calculated as the sum of the scores from all four paws. Three days after the final administration, the paw morphology of mice was photographed. Subsequently, the mice were euthanized to collect serum, ankles, and major organs. Animal experiments were permitted by the Experimental Animal Ethics Committee of Yangzhou University (No.202408037).

2.16. In vivo biodistribution

Another six DBA/1J mice were purchased to observe the biodistribution of nanomaterials *in vivo*. The same method was used to construct a collagen-induced RA model. Subsequently, FITC-labelled siRNA and EM/siKEAP1@Fe-MOF@HA (1.5 mg/kg) were injected via

the tail vein. At 1, 8, and 24 h of injection, the fluorescence distribution was observed and recorded using a *in vivo* optical imaging system (IVIS Lumina III, PerkinElmer). Meanwhile, one mouse in each group was executed at 1, 8, and 24 h, respectively, to observe the fluorescence distribution in the major organs.

2.17. Hematoxylin & eosin (H&E) staining

The prepared ankle tissue sections were routinely dewaxed and hydrated, and stained according to the H&E staining kit (C0105S, Beyotime) instructions. Specifically, hematoxylin was first dropped into the sections for 5 min of staining. After rinsing with running water, slices were then dehydrated in alcohol and stained with eosin for 1–2 min. After washing and dehydrating again, the sections were sealed for image acquisition using the microscopy.

2.18. Safranin O staining

The infiltration of immune cells was observed using a Safranin O staining kit (G1371, Solarbio). The tissue sections were pretreated and subsequently stained by fresh Weigert's staining solution for 3–5 min. After washing, the sections were impregnated with solid green staining solution for 5 min. Following, these sections were washed with a weak acid solution and treated by the saffron staining solution for 5 min. After dehydration and sealing, the sections were imaged using a microscope.

2.19. Terminal deoxynucleotidyl transferase (TdT)-mediated dUTP nick-end labelling (TUNEL)

TUNEL Assay Kit (C1086, Beyotime) was used to detect the apoptosis in ankle tissues. Briefly, 50 μL of prepared proteinase K working solution was added dropwise to the dewaxed and hydrated tissue sections for a 30-min digestion. After rinsing, configured TUNEL working solution was added to sections and incubated for 1 h away from light, followed by the DAPI staining for 10 min. Ultimately, washed sections were blocked with an anti-fluorescence quenching sealing solution and placed under a microscope for observation.

2.20. In vivo biosafety assessment

To assess the biosafety of nanoparticles, fresh blood was collected from each group of mice. Blood coagulation was allowed for 30 min at room temperature, and centrifuged at 2000×*g* for 10 min. Serum appeared in the upper layer of yellow clarified liquid was assayed for the levels of liver function (aspartate transaminase [AST] and alanine transaminase [ALT]) and kidney function (creatinine [Cre] and blood urea nitrogen [BUN]) indexes using an automatic biochemical analyzer (Indiko, Thermo Scientific). Meanwhile, heart, liver, spleen, lung, and kidney tissues were also collected from each group of mice and evaluated for their pathological features by H&E staining as described previously.

2.21. Statistical analysis

All data were presented as mean ± standard deviation and processed for statistical analysis in GraphPad 10.1.2. Differences between two groups were compared using unpaired *t* tests. The One-way analysis of variance (ANOVA) and Tukey's post hoc test were implemented for comparison between groups. Comparisons between multiple groups at consecutive times were analyzed by two-way repeated measure ANOVA. Results achieving $P < 0.05$ were defined as statistical significance.

3. Results

3.1. Synthesis and physicochemical properties evaluation of nanoparticles

In this study, EM and siKEAP1 were loaded into the Fe-MOF voids by free diffusion and electrostatic adsorption, respectively. To avoid drug degradation during delivery and to ensure the targeting of nanoparticles to macrophages, EM/siKEAP1@Fe-MOF was further encapsulated by HA. The nanomaterial synthesis and preparation process are shown in Fig. 2A. Subsequently, nanoparticles were characterized to confirm their successful preparations. Results of FTIR indicated that the characteristic peaks of Fe-MOF group at 3421 cm^{-1} are the stretching vibration peaks of N-H in the amino group and O-H in the carboxyl group. Meanwhile, the absorption peaks appearing at 1627, 1382, 710, and 461 cm^{-1} correspond to the characteristics of C=O, C-O, aryl-ring C-H, and Fe-O functional groups in Fe-MOF, respectively. The characteristic peaks observed at 1623, 1481, 133, and 1270 cm^{-1} in the EM group are attributed to the carbonyl C=O stretching vibration, C-C aromatic stretching vibration, -OH bending vibration, and C-O stretching vibration, respectively. EM@Fe-MOF not only retained the basic characteristic peak of Fe-MOF frame (characteristic peak at 461 cm^{-1} for Fe-O), but also displayed the absorption peak of EM in the range of 1000–1500 cm^{-1}, indicating that EM was successfully encapsulated in the framework of Fe-MOF. In addition, EM@Fe-MOF@HA experienced an anti-symmetric surface exocyclic stretching vibration of sugar at 1038 cm^{-1}, demonstrating the successful wrapping of HA (Fig. 2B). Under TEM, EM/siKEAP1@Fe-MOF@HA showed the polyhedral morphology with larger particle size and blurring edges compared with Fe-MOF and Fe-MOF@HA (Fig. 2C). The N_2 absorption results suggested a progressive decrease in N_2 uptake of Fe-MOF@HA and EM/siKEAP1@Fe-MOF@HA compared to Fe-MOF (Fig. 2D), suggesting that the loading of EM and siKEAP1 resulted in the reduction of material voids to prevent the entry of N_2. During the preparation process, the positive charge carried by Fe-MOF and EM conferred the possibility for siKEAP1 and HA to be electrostatically adsorbed onto the surface of nanoparticles and leaded to a decrease in the zeta potential of EM/siKEAP1@Fe-MOF@HA (Fig. 2E). EM/siKEAP1@Fe-MOF@HA also showed increased particle size from 161.9 nm of Fe-MOF and 190.6 nm of Fe-MOF@HA to finally 207.5 nm (Fig. 2F).

In EM/siKEAP1@Fe-MOF@HA, the loading efficiency of EM and siKEAP1 reached 23.85 % and 9.85 %, respectively. Meanwhile, the complexation ability of EM@Fe-MOF to siKEAP1 under different N/P ratios was tested using AGE. The results demonstrated that with the increase of N/P ratio, the fluorescence intensity of siRNA bands gradually decreased but completely disappeared at 20:1, suggesting a complete migration of siRNA and full adsorption between EM@Fe-MOF and siKEAP1 at N/P = 20:1 (Fig. 2G). When EM/siKEAP1@Fe-MOF@HA was dispersed in PBS or FBS, its particle size and PDI showed no significant changes within 144 h, suggesting the stability of nanoparticles *in vitro* (Fig. 2H). Meanwhile, the release of EM and siKEAP1 from EM/siKEAP1@Fe-MOF@HA at pH 5.4 was significantly higher than that at pH 7.4, and gradually remained stable after reaching about 60 % at 36 h (Fig. 2I). The above results suggested that the EM/siKEAP1@Fe-MOF@HA co-delivery system was successfully constructed and characterized by stable physicochemical and pH-responsive properties.

3.2. In vitro intracellular uptake

The degradable and biocompatible HA can bind CD44 receptors on macrophage membranes, thus endowing nanoparticles with targeting properties [25,26]. To confirm the targeting of EM/siKEAP1@Fe-MOF@HA to macrophages, activated RAW264.7 and THP-1 cells were treated with nanoparticles. qPCR results suggested a remarkable elevation of TNF-α, IL-1β, and IL-6 levels, but the addition of EM/siKEAP1@Fe-MOF@ HA significantly reversed the upregulation of these inflammatory cytokines (Fig. 3A). Using flow cytometry, we

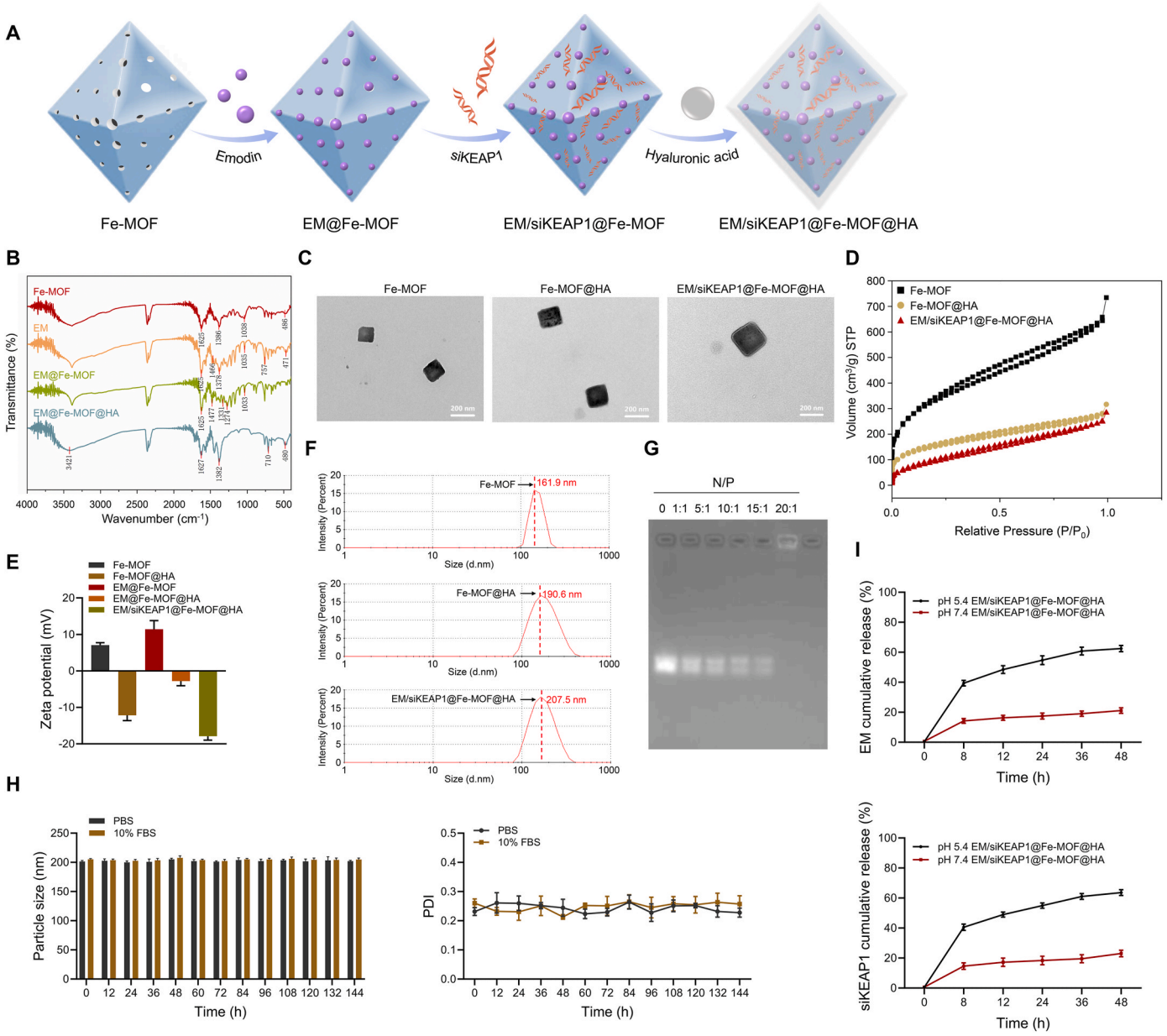

Fig. 2. Characterization of nanoparticles.
(A) Schematic illustration of the construction of nanoparticles. (B) FTIR reveals structurally characterized peaks of each group of nanoparticles. (C) TEM for the observation of micromorphology of Fe-MOF, Fe-MOF@HA, and EM/siKEAP1@Fe-MOF@HA. Scale bar = 200 nm. (D) N_2 uptake of Fe-MOF, Fe-MOF@HA, and EM/siKEAP1@Fe-MOF@HA. (E–F) Zeta potential (E) and particle size (F) of nanoparticles. (G) Migration block of siKEAP1 under different N/P ratios. (H) Changes in particle size and PDI of EM/siKEAP1@Fe-MOF@HA dispersed in PBS and 10 %FBS within 144 h. (I) The release difference of EM and siKEAP1 between pH5.4 and 7.4. All experimental data were derived from three independent replicates.

observed that the uptake of EM/siKEAP1@Fe-MOF@HA by activated macrophages was significantly higher than that by inactivated ones (Fig. 3B). More importantly, intracellular uptake of EM/siKEAP1@Fe-MOF@HA demonstrated a significant time-dependent increase (Fig. 3C). These findings revealed that EM/siKEAP1@Fe-MOF@HA can target activated macrophages to promote its intracellular uptake.

To explore the detailed uptake mechanism, we pretreated the cells with nystatin, CPZ, and colchicine, which inhibited the endocytosis mediated by caveolin, clathrin and micropinocytosis, respectively [27,28]. The results suggested that these inhibitors could reduce the cellular uptake of EM/siKEAP1@Fe-MOF@HA, with CPZ demonstrating the most pronounced inhibitory effect (Fig. 3D). Therefore, EM/siKEAP1@Fe-MOF@HA may be internalized by macrophages through clathrin-mediated endocytosis.

3.3. *Pro-polarization in macrophages and anti-inflammation effects of nanoparticles in vitro*

To further probe into effects of EM/siKEAP1@Fe-MOF@HA on macrophage function, a series *in vitro* experiments were conducted. The treatment with EM/siKEAP1@Fe-MOF@HA did not induce significant differences in proliferation between activated and inactivated macrophages. However, it was observed that 10 μg/mL of EM/siKEAP1@Fe-MOF@HA exhibited the most pronounced inhibitory effect on macrophage proliferation, and therefore was selected as the optimal dose for subsequent experiments (Fig. 4A). More importantly, nanoparticles loaded with EM and siKEAP1 significantly inhibited the expression of

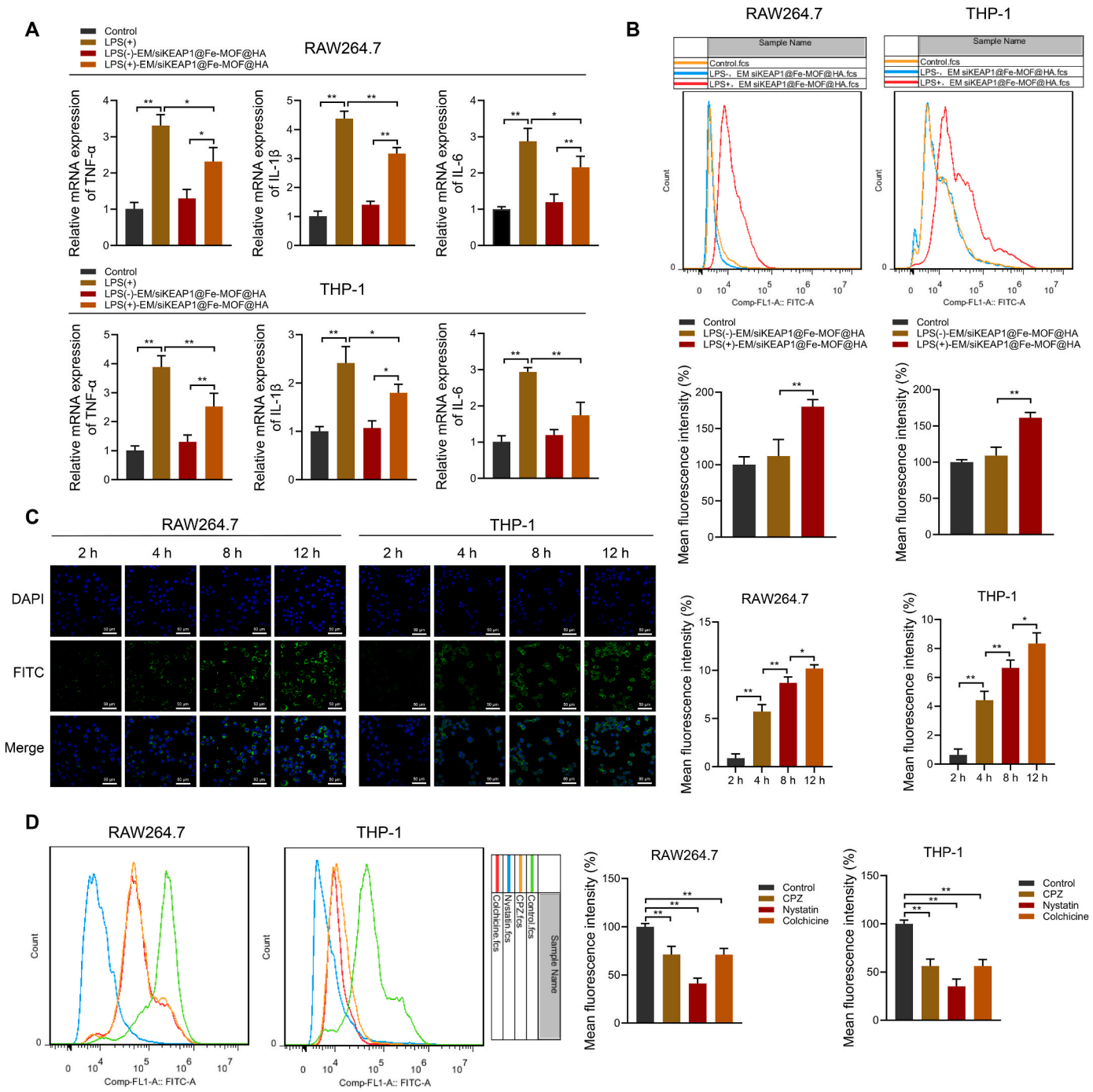

Fig. 3. Intracellular uptake of EM/siKEAP1@Fe-MOF@HA and its mechanism.
(A) Levels of TNF-α, IL-1β, and IL-6 in macrophages treated with LPS and/or EM/siKEAP1@Fe-MOF@HA. (B) Differences in uptake of EM/siKEAP1@Fe-MOF@HA before and after the activation of macrophages. (C) CLSM revealed the difference of EM/siKEAP1@Fe-MOF@HA uptake by activated macrophages at different times. Scale bar = 50 μm. (D) Uptake difference of EM/siKEAP1@Fe-MOF@HA by macrophages treated with different inhibitors. All experimental data were derived from three independent replicates for statistical analysis. $*P < 0.05$; $**P < 0.01$.

polarization markers of M1 macrophage (iNOS and IL-1β), while promoting M2 phenotype markers (Arg-1 and CD206) expression to a greater extent than free EM, free KEAP1, and EM- or siKEAP1-loaded Fe-MOF@HA (Fig. 4B and C). Furthermore, EM/siKEAP1@Fe-MOF@HA could significantly reduce the levels of pro-inflammatory product NO and pro-inflammatory factor IL-6 and TNF-α (Fig. 5A and B), inhibit the mRNA and protein expression of KEAP1 (Fig. 5C and D), enhance the protein level of downstream Nrf2 (Fig. 5D), and block the generation of intracellular ROS (Fig. 5E), with superior efficacy compared to the other treatment groups. Therefore, EM/siKEAP1@Fe-MOF@HA exerts anti-inflammatory and antioxidant effects by mediating KEAP1/Nrf2 axis and promoting macrophage polarization *in vitro*.

3.4. *In vivo biodistribution and anti-RA effects of nanoparticles*

To clarify the therapeutic efficacy of EM/siKEAP1@Fe-MOF@HA on RA, a collagen-induced RA model was constructed in this study. The schedule for animal experiments is detailed in Fig. 6A. By labelling with

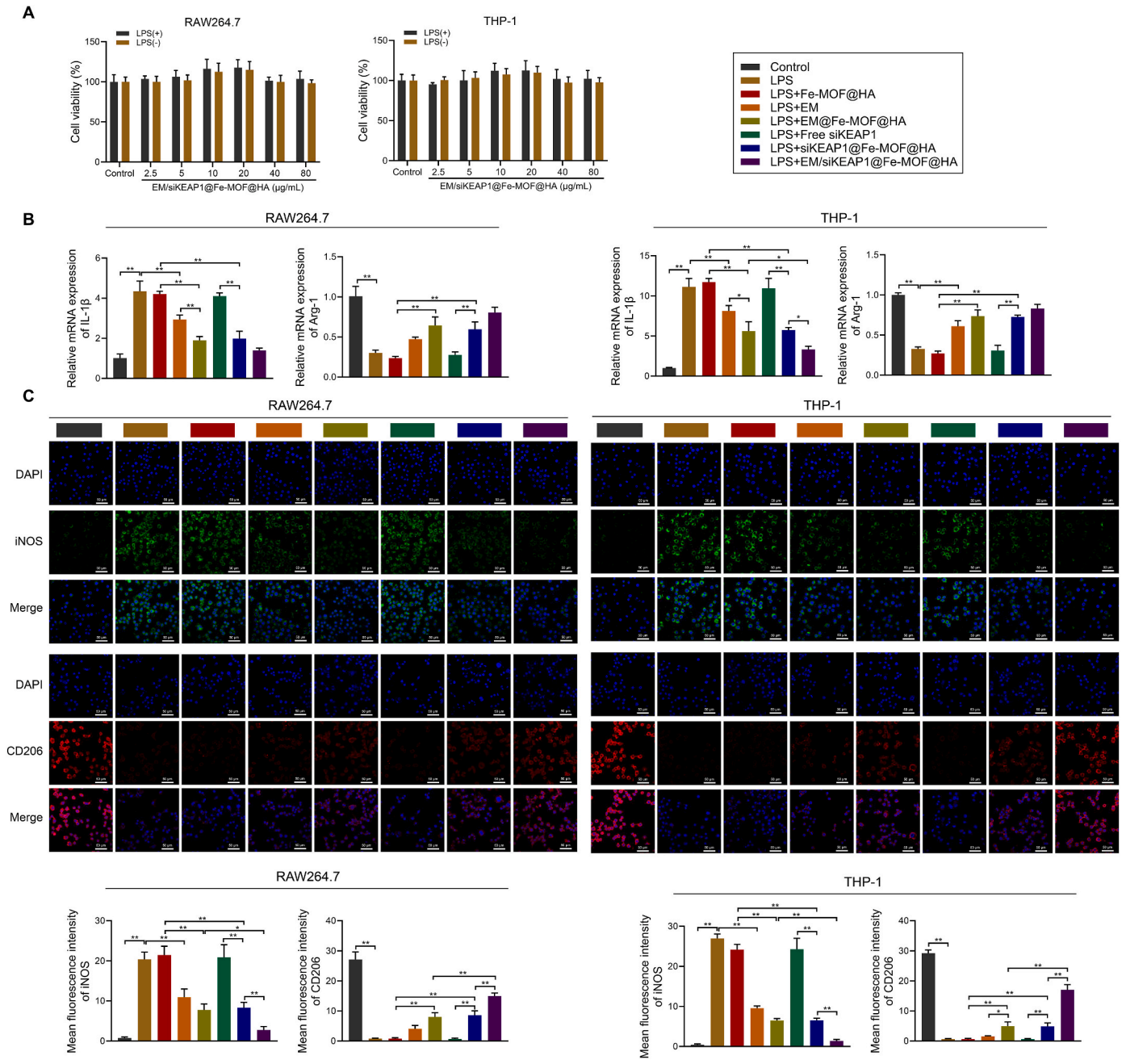

Fig. 4. Internalization of EM/siKEAP1@Fe-MOF@HA affected macrophage polarization.
(A) Effects of EM/siKEAP1@Fe-MOF@HA on macrophage proliferation under different concentrations (n = 4). (B) The mRNA expression levels of M1 phenotypic marker IL-1β and M2 phenotypic marker Arg-1 under nanoparticle treatment (n = 3). (C) The protein expression levels of M1 phenotypic marker iNOS and M2 phenotypic marker CD206 under nanoparticle treatment (n = 3). Scale bar = 50 μm *$P < 0.05$; **$P < 0.01$.

FITC, the biodistribution of nanoparticles was observed using the *in vivo* imaging. It was found that EM/siKEAP1@Fe-MOF@HA was more distributed in the inflammation lesions of mice compared with free siKEAP1, and its fluorescence intensity reached the maximum at 8 h (Fig. 6B). In *ex vivo* tissue analysis, fluorescence was predominantly localized in the liver and kidneys, indicating a preferential accumulation of the administered agent in these organs. In contrast, no detectable fluorescence was observed in the heart, spleen, or lungs (Fig. 6C). EM/siKEAP1@Fe-MOF@HA also significantly reduced the expression of KEAP1 mRNA and protein levels in the ankle tissues of mice with the prolongation of time (Fig. 6D and E). Thus, the modification of siKEAP1 with nanoparticles can promote its internalization in macrophages, thus achieving the downregulation of KEAP1. In terms of therapeutic effect, the treatment with EM/siKEAP1@Fe-MOF@HA could significantly reduce paw thickness and clinical score of RA mice, compared with EM@Fe-MOF@HA and siKEAP1@Fe-MOF@HA treatment groups (Fig. 6F). To further observe the histopathologic morphology, immune cell infiltration, and articular cartilage structure in ankle joint, H&E and Safranin O staining were carried out in this study. The results suggested that the ankle joint of mice in the model group showed severe bone erosion and inflammation, with reduced articular cartilage. After EM/siKEAP1@Fe-MOF@HA treatment, the joints of mice showed a complete smooth surface and increased articular cartilage content, without obvious bone erosion and inflammatory cell infiltration (Fig. 6G). Furthermore, the significantly elevated ankle apoptotic rate in the model group was markedly reversed after undergoing treatment with

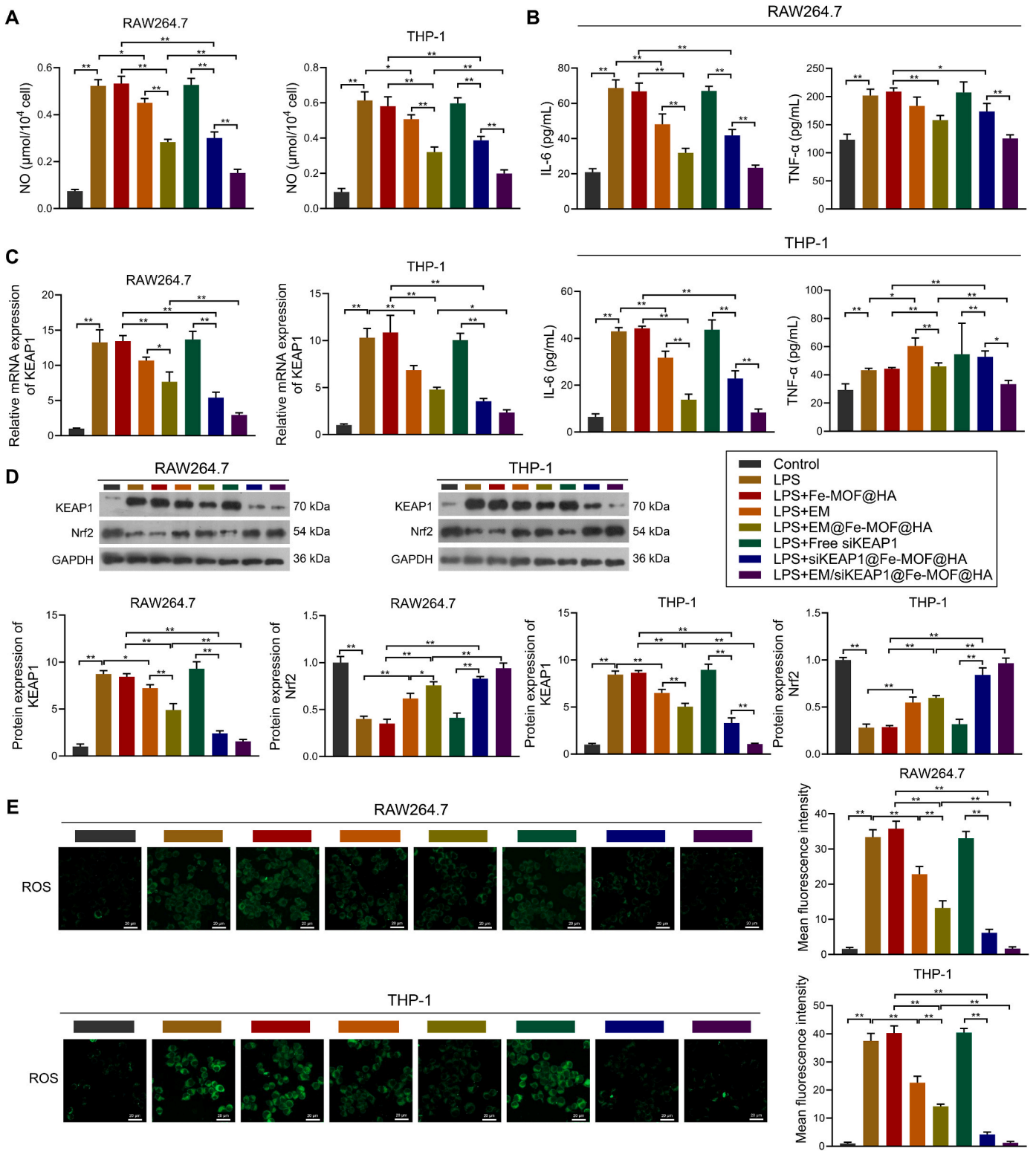

Fig. 5. EM/siKEAP1@Fe-MOF@HA exerted anti-inflammatory and antioxidant effects in macrophages.
(A–E) Effects of nanoparticle internalization on the levels of pro-inflammatory product NO (A), the secretion of inflammatory factors (B), the mRNA level of KEAP1 (C), the protein expression of KEAP1 and its downstream target Nrf2 (D), and the generation of intracellular ROS (E) in macrophages. Scale bar = 20 μm. All experimental data were derived from three independent replicates for statistical analysis. $^{*}P < 0.05$; $^{**}P < 0.01$.

EM/siKEAP1@Fe-MOF@HA, whose inhibition efficiency was superior to that of the EM@Fe-MOF@HA and siKEAP1@Fe-MOF@HA groups (Fig. 6H).

3.5. *Macrophage-mediated protective effects of nanoparticles on the inflammatory in vivo*

This study further evaluated effects of the nanoparticle internalization on inflammatory factors and polarization markers in macrophages.

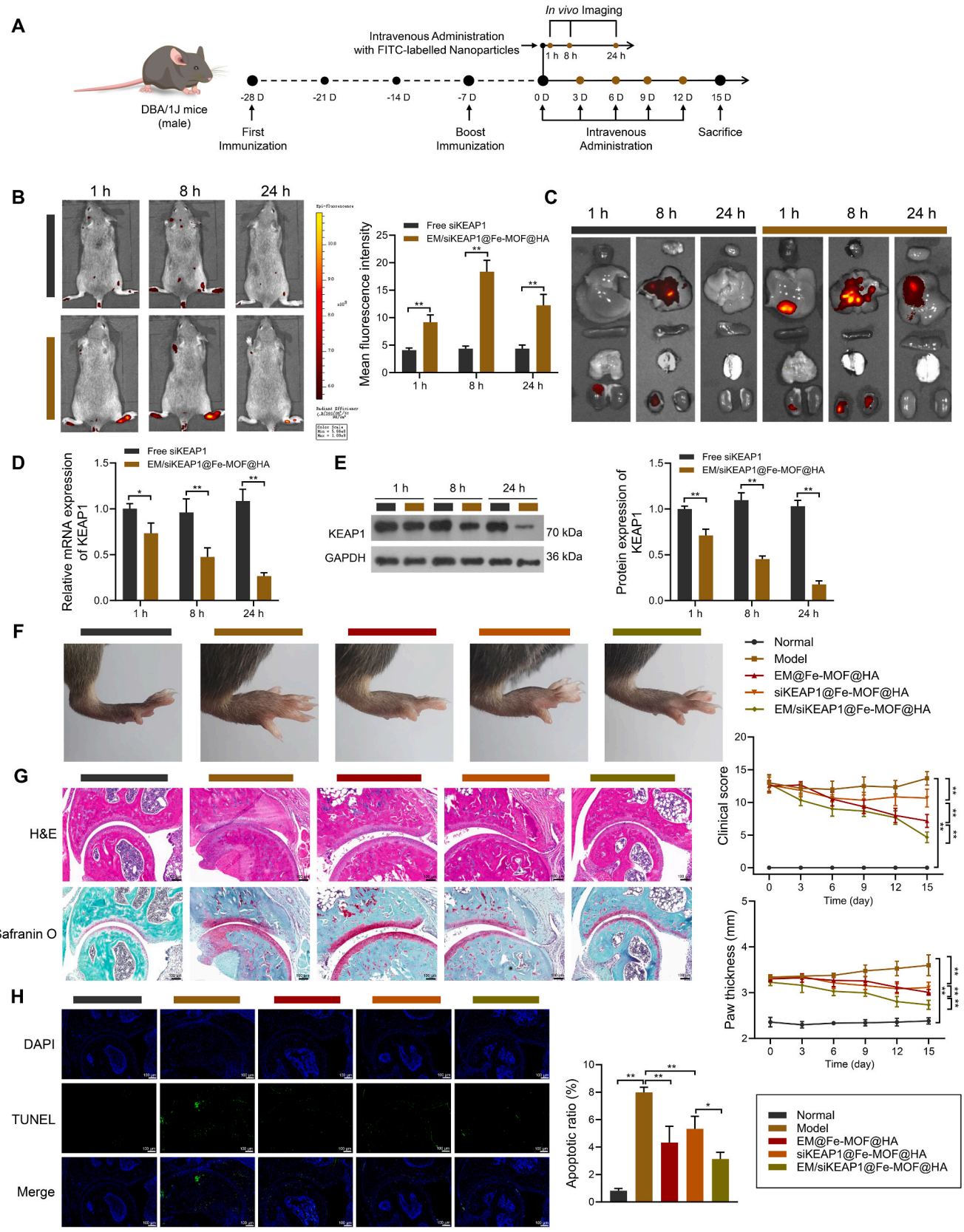

Fig. 6. Efficacy evaluation of nanomaterials for RA therapy *in vivo*.
(A) The overall schedule for therapeutic efficacy evaluation of nanoparticles. (B) *In vivo* biodistribution of nanoparticles (n = 3). (C) Fluorescence distribution in major organs (heart, liver, spleen, lung, and kidney) (n = 3). (D–E) The KEAP1 mRNA (D) and protein (E) expression levels in mice ankle tissues with the treatment of nanoparticles (n = 3). (F) Effect nanomaterials on paw thickness and clinical score in mice (n = 6). (G) H&E and Safranin O staining showed the effects of drug co-delivery nanosystem on the tissue morphology and cartilage content of ankle joint in mice, respectively (n = 3). Scale bar = 100 μm. (H) Effect of nanomaterials on apoptosis of ankle joint tissue in mice (n = 3). Scale bar = 100 μm $^{*}P < 0.05$; $^{**}P < 0.01$.

The treatment with EM/siKEAP1@Fe-MOF@HA significantly downregulated the mRNA and protein levels of KEAP1 but increased the protein expression of its downstream target Nrf2 in the ankle tissues of RA mice, compared with EM@Fe-MOF@HA and siKEAP1@Fe-MOF@HA (Fig. 7A and B). Furthermore, EM/siKEAP1@Fe-MOF@HA also significantly suppressed the levels of inflammatory factors (IL-6 and TNF-α) and expression of macrophage M1 phenotypic markers (IL-1β and iNOS) in ankle tissues of RA mice, while promoting the expression of M2 phenotypic markers (Arg-1 and CD206) compared with other treatment groups (Fig. 7C and D). The above findings illustrated that EM/siKEAP1@Fe-MOF@HA ameliorated the inflammatory response and promoted macrophage polarization in the ankle tissues of RA mice.

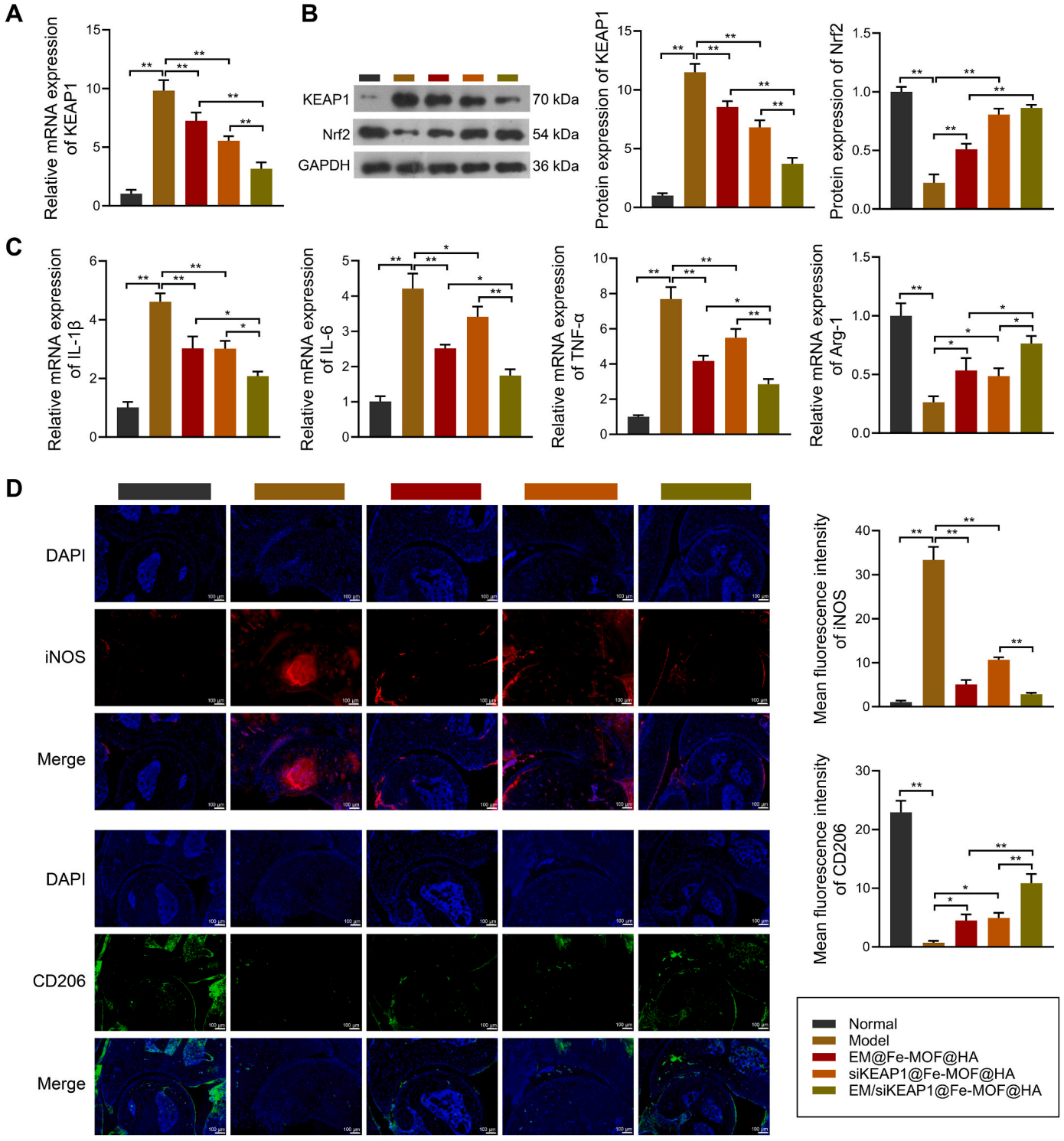

Fig. 7. Effects of nanoparticle internalization on inflammatory factors and polarization markers in macrophages.
(A–B) Alterations in the mRNA level of KEAP1, and the protein expression of KEAP1 and Nrf2 (B) in ankle tissues of RA mice under different treatment groups. (C–D) Differences in expression levels of inflammatory factor (C) and macrophage polarization markers (D) among ankle tissues of RA mice treated with different groups of nanoparticles. Scale bar = 100 μm. All experimental data were derived from three independent replicates for statistical analysis. *$P < 0.05$; **$P < 0.01$.

3.6. Assessment of biosafety in vivo

The biosafety of nanoparticles *in vivo* was evaluated by histologic observations of major organs and tests of liver and kidney functions. The body weight of mice in the treatment group exhibited a stable and consistent increase over the experimental period (Fig. 8A), suggesting a controlled cytotoxicity of nanoparticles. Subsequently, H&E staining was carried out to observe the morphology of major organs and showed no obvious immune cell infiltration and structure differences in heart, liver, spleen, lung and kidney tissues between groups (Fig. 8B). Detection for serum levels of ALT, AST, BUN, and Cre also indicated no significant differences in liver and kidney functions among the groups (Fig. 8C). Therefore, it can be concluded that the nanoparticles possess an optimistic biosafety *in vivo*.

4. Discussion

This study successfully loaded EM and siKEAP1 in Fe-MOF by free diffusion and electrostatic adsorption, and the drug loading efficiency of EM and siKEAP1 could reach 23.85 % and 9.85 %, respectively. After further encapsulation of HA, the nanoparticles not only had stable physicochemical properties, but also responded to pH and accelerated the release of drugs under acidic conditions. In RA pathology, oxidative stress is involved in disease progression through DNA damage and lipid metabolism, a process that is accompanied by lactate production and pH reduction [29]. In acidic environments, both HA and Fe-MOF can effectively decompose and release inclusions to function as drug delivery carriers [19,30]. In addition, the specific binding of HA to CD44 receptor confers the ability of nanoparticles to target macrophages. It has been demonstrated that the modification with HA enhances the binding of ligand to CD44 receptor, a surface receptor on M1 macrophages, thereby improving the targeting of nanoparticles to macrophages in the inflammatory lesions of RA [31,32]. As expected, this study confirmed the inflammatory targeting of EM/siKEAP1@Fe-MOF@HA and its specific uptake in macrophages by cell- and animal-based experiments. Furthermore, we also found that EM/siKEAP1@Fe-MOF@HA may be internalized by macrophages mainly by clathrin-mediated endocytosis, which was in agreement with other therapeutic nanoparticles for alleviating RA inflammation by targeting macrophages [33]. Therefore, EM/siKEAP1@Fe-MOF@HA exerted its anti-RA effects by targeting macrophages. These findings also provide a foundation for elucidating the mechanisms underlying macrophage polarization.

In this study, after co-delivery of EM and siKEAP1, the nanomaterial observably reduced the levels of inflammatory cytokines, pro-inflammatory product NO, and intracellular ROS, and promoted the polarization of macrophages both *in vitro* and *in vivo*. Among them, TNF-α and IL-6 are secreted by macrophage pro-inflammatory M1 phenotype for maintaining inflammation in RA [6,34]. The significant reduction in NO levels in macrophages may be attributed to the elimination of RONS precursors, which serve as a hallmark of M1-polarized macrophages and trigger the inflammation responses in RA [35]. Consistent with findings of the present study, Zhu et al. proposed that EM may inhibit LPS-induced inflammation through the inactivation of PPARγ-dependent NF-κB pathway [36]. During the treatment of RA, EM may also suppress the production and delivery of inflammatory factors by affecting macrophage subpopulation aggregation and exosome secretion [37]. However, as mentioned previously, the balance of M1/M2 macrophage phenotype is crucial for alleviating RA joint inflammation [38,39]. Our findings suggested that the treatment with EM significantly promoted macrophage polarization, as evidenced by the down-regulation of M1 phenotypic markers and upregulation of M2

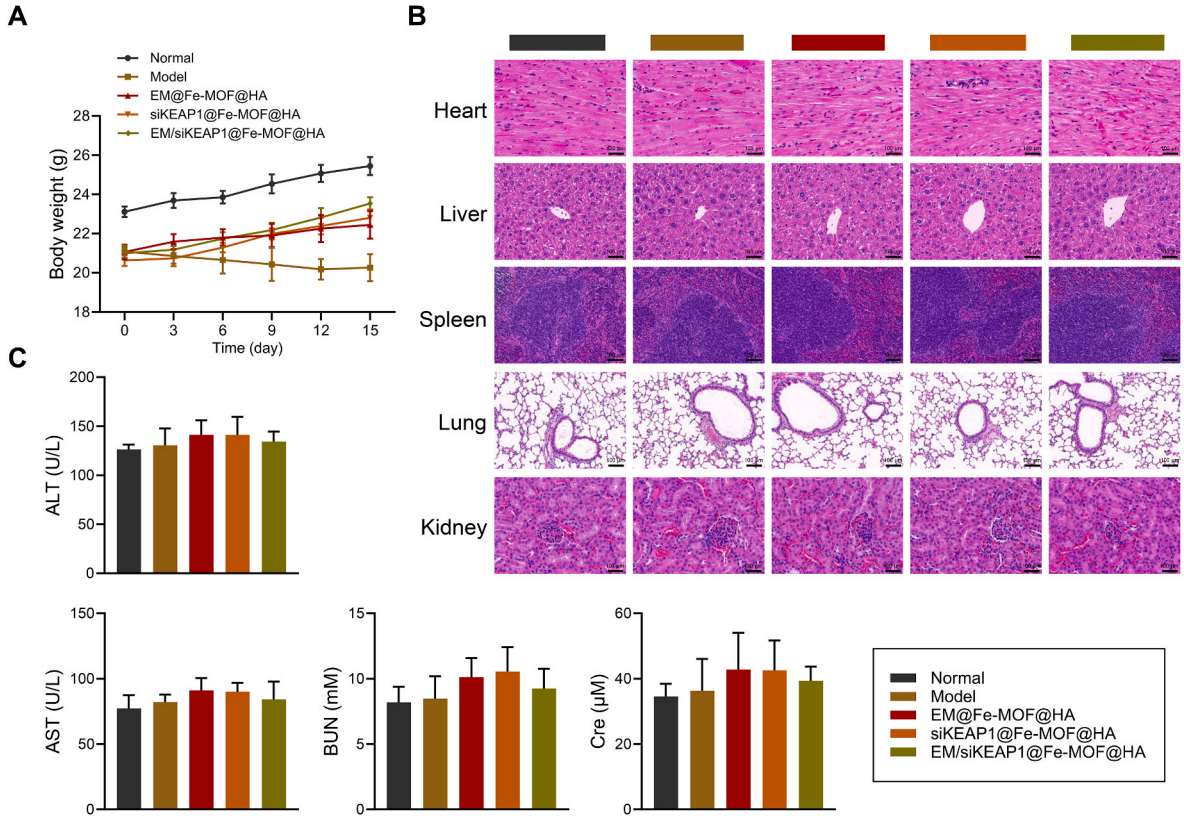

Fig. 8. Biosafety evaluation of nanoparticles *in vivo*.
(A) Body weight of mice in model and treatment groups at different time points (n = 6). (B) HE staining showed the morphology of heart, liver, spleen, lung, and kidney tissues of each group of mice (n = 3). Scale bar = 100 μm. (C) Serum levels of liver function (ALT and AST) and renal function (BUN and Cre) indexes in model and treatment groups (n = 6).

phenotypic markers. Mechanistically, EM may promote the proportion of anti-inflammatory M2 macrophage through inhibition of p65-NF-κB complex [40]. EM may also inhibit chronic inflammation in obese mice *in vivo* by promoting M2 macrophage polarization via TREM2 [41]. The EM-mediated cAMP/PKA pathway contributes to macrophage polarization regulation and inflammatory resistance in acute lung injury [42]. Although the involvement of these pathways has not been elucidated in this study, above findings support a potential molecular mechanism of macrophage polarization during EM treatment against RA and provide clues for subsequent studies.

Similar to EM, siKEAP1 also demonstrated pro-macrophage polarization and anti-inflammatory potentials in the present study. More importantly, EM was able to down-regulate KEAP1 expression and alleviate acute kidney injury by activating the Nrf2 pathway [43]. KEAP1-mediated Nrf2/ARE pathway is also involved in the mechanism by which DANCR promotes inflammation and oxidative stress in RA [44]. The Nrf2/KEAP1 pathway is a conserved intracellular defense mechanism that responds to inflammatory stimulators and corrects for deviations from endogenous homeostasis [45]. The cytoprotective Nrf2/KEAP1 signaling pathway has been found to involve in the protection against inflammatory responses, oxidative stress, and migration of fibroblast-like synoviocytes in RA [46,47]. Specifically, KEAP1 is a negative regulator of Nrf2, whose activation suppresses autoimmune arthritis in mice by inhibiting the expression of pro-inflammatory cytokines and inducing the expression of antioxidant enzymes [48]. The regulation of KEAP1 on macrophage polarization is also dependent on Nrf2. It was found that the destruction of KEAP1-specific sites can reduce the binding of KEAP1 to Nrf2, thereby allowing the migration of Nrf2 to the nucleus and inhibiting the polarization towards M1 macrophages [49]. Consistent with these findings, our results demonstrated that the synthesized nanoparticles effectively suppressed KEAP1 expression while upregulating the protein level of Nrf2. We therefore speculated that the internalization of siKEAP1 in macrophages may activate Nrf2-mediated cytoprotective mechanisms and reinforce anti-inflammatory effects in RA therapy.

However, high doses and prolonged EM use may induce reproductive toxicity, which was not discussed in this study. Furthermore, the extensive production of glucuronidation by EM may reduce its oral bioavailability in rats [50]. Therefore, pharmacokinetic testing of EM/SiKEAP1@Fe-MOF@HA is still required to determine its reproductive toxicity and specific route of administration before the clinical application.

5. Conclusion

In this study, HA-coated EM/siKEAP1@Fe-MOF not only had stable physicochemical properties, but also specifically targeted macrophages to enhance its internalization. This nanosystem co-delivering EM and siKEAP1 ensured biosafety *in vivo*, while effectively suppressing the inflammatory response and ameliorating the RA pathology by inducing the macrophage polarization towards M2 phenotype. Therefore, EM/siKEAP1@Fe-MOF@HA is expected to become a new approach for RA treatment and be applied in the biomedical field.

CRediT authorship contribution statement

Muting Qin: Writing – original draft, Visualization, Funding acquisition, Formal analysis, Data curation, Conceptualization. **Penglu Chen:** Writing – original draft, Visualization, Formal analysis, Data curation, Conceptualization. **Huanxue Chen:** Writing – original draft, Visualization, Formal analysis, Data curation. **Feng Liu:** Software, Methodology, Formal analysis. **Wei He:** Writing – review & editing. **Enyang Yao:** Writing – review & editing, Methodology, Conceptualization.

Ethics approval

Animal experiments were permitted by the Experimental Animal Ethics Committee of Yangzhou University (No.202408037).

Funding statement

This work was supported by Scientific Research Project of Higher Education Institutions in Liaoning Province (LQNK201708).

Declaration of competing interest

The authors declare that they have no known competing financial interests or personal relationships that could have appeared to influence the work reported in this paper.

Acknowledgements

This work was supported by the Scientific Research Project of Higher Education Institutions in Liaoning Province (Grant No. LQNK201708). We are grateful to the Experimental Animal Ethics Committee of Yangzhou University for approving the animal experiments (Approval No. 202408037).

Data availability

Data will be made available on request.

References

[1] P. Brown, A.G. Pratt, K.L. Hyrich, Therapeutic advances in rheumatoid arthritis, BMJ (Clin. Res. Ed.) 384 (2024) e070856.
[2] J.J. Cush, Rheumatoid arthritis: early diagnosis and treatment, Rheum. Dis. Clin. N. Am. 48 (2) (2022) 537–547.
[3] E. Peterson, M.K. Gallagher, J. Wilbur, Rheumatoid arthritis: diagnosis and management for the family physician, Am. Fam. Physician 110 (5) (2024) 515–526.
[4] M. Cutolo, R. Campitiello, E. Gotelli, S. Soldano, The role of M1/M2 macrophage polarization in rheumatoid arthritis synovitis, Front. Immunol. 13 (2022) 867260.
[5] S. Jang, E.J. Kwon, J.J. Lee, Rheumatoid arthritis: pathogenic roles of diverse immune cells, Int. J. Mol. Sci. 23 (2) (2022).
[6] Y. Zheng, K. Wei, P. Jiang, J. Zhao, Y. Shan, Y. Shi, F. Zhao, C. Chang, Y. Li, M. Zhou, X. Lv, S. Guo, D. He, Macrophage polarization in rheumatoid arthritis: signaling pathways, metabolic reprogramming, and crosstalk with synovial fibroblasts, Front. Immunol. 15 (2024) 1394108.
[7] H. Li, Y. Feng, X. Zheng, M. Jia, Z. Mei, Y. Wang, Z. Zhang, M. Zhou, C. Li, M2-type exosomes nanoparticles for rheumatoid arthritis therapy via macrophage re-polarization, J. Contr. Release 341 (2022) 16–30.
[8] A. Di Matteo, J.M. Bathon, P. Emery, Rheumatoid arthritis, Lancet (London, England) 402 (10416) (2023) 2019–2033.
[9] A.F. Radu, S.G. Bungau, Management of rheumatoid arthritis: an overview, Cells 10 (11) (2021).
[10] Q. Zhang, W.W. Chen, X. Sun, D. Qian, D.D. Tang, L.L. Zhang, M.Y. Li, L.Y. Wang, C.J. Wu, W. Peng, The versatile emodin: a natural easily acquired anthraquinone possesses promising anticancer properties against a variety of cancers, Int. J. Biol. Sci. 18 (8) (2022) 3498–3527.
[11] R.B. Semwal, D.K. Semwal, S. Combrinck, A. Viljoen, Emodin - a natural anthraquinone derivative with diverse pharmacological activities, Phytochemistry 190 (2021) 112854.
[12] N. Luo, J. Fang, L. Wei, A. Sahebkar, P.J. Little, S. Xu, C. Luo, G. Li, Emodin in atherosclerosis prevention: pharmacological actions and therapeutic potential, Eur. J. Pharmacol. 890 (2021) 173617.
[13] M. Zhu, K. Yuan, Q. Lu, Q. Zhu, S. Zhang, X. Li, L. Zhao, H. Wang, G. Luo, T. Wang, G. Huang, A. Xu, Emodin ameliorates rheumatoid arthritis by promoting neutrophil apoptosis and inhibiting neutrophil extracellular trap formation, Mol. Immunol. 112 (2019) 188–197.
[14] L. Cheng, J. Chen, X. Rong, Mechanism of emodin in the treatment of rheumatoid arthritis, Evid. base Compl. Alternative Med. : eCAM 2022 (2022) 9482570.
[15] Y. Zhang, G. Wang, T. Wang, W. Cao, L. Zhang, X. Chen, Nrf2-Keap1 pathway-mediated effects of resveratrol on oxidative stress and apoptosis in hydrogen peroxide-treated rheumatoid arthritis fibroblast-like synoviocytes, Ann. N. Y. Acad. Sci. 1457 (1) (2019) 166–178.
[16] L. Tang, M. Li, S. Piao, L. Du, S. Qiu, X. Jiang, M. Luo, Y. Wang, Z. Pan, Activation of the Keap1/Nrf2/HO-1 pathway by "Tianyu" pairing: implications for inflammation and oxidative stress in rheumatoid arthritis, Endocr. Metab. Immune Disord. - Drug Targets (2024).

[17] L. Chen, D. Zhao, X. Ren, J. Ren, X. Meng, C. Fu, X. Li, Shikonin-loaded hollow Fe-MOF nanoparticles for enhanced microwave thermal therapy, ACS Biomater. Sci. Eng. 9 (9) (2023) 5405–5417.
[18] A.K.K. Padinjareveetil, J.V. Perales-Rondon, D. Zaoralová, M. Otyepka, O. Alduhaish, M. Pumera, Fe-MOF catalytic nanoarchitectonic toward electrochemical ammonia production, ACS Appl. Mater. Interfaces 15 (40) (2023) 47294–47306.
[19] J.J. Shen, S.J. Xue, Z.H. Mei, T.T. Li, H.F. Li, X.F. Zhuang, L.M. Pan, Synthesis, characterization, and efficacy evaluation of a PH-responsive Fe-MOF@GO composite drug delivery system for the treating colorectal cancer, Heliyon 10 (6) (2024) e28066.
[20] R.V. Pinto, C.C. Cao, P. Lyu, I. Dovgaliuk, W. Shepard, E. Rivière, C.Y. Su, G. Maurin, F. Antunes, J. Pires, V. André, C. Henriques, A. Tissot, M.L. Pinto, C. Serre, Ultra-microporous Fe-MOF with prolonged NO delivery in biological media for therapeutic application, Small 20 (48) (2024) e2405649.
[21] Y. Zhong, W. Liu, C. Rao, B. Li, X. Wang, D. Liu, Y. Pan, J. Liu, Recent advances in Fe-MOF compositions for biomedical applications, Curr. Med. Chem. 28 (30) (2021) 6179–6198.
[22] L. Guo, S. Zhong, P. Liu, M. Guo, J. Ding, W. Zhou, Radicals scavenging MOFs enabling targeting delivery of siRNA for rheumatoid arthritis therapy, Small 18 (27) (2022) e2202604.
[23] P. Wang, Y. Zhang, H. Lei, J. Yu, Q. Zhou, X. Shi, Y. Zhu, D. Zhang, P. Zhang, K. Wang, K. Dong, J. Xing, Y. Dong, Hyaluronic acid-based M1 macrophage targeting and environmental responsive drug releasing nanoparticle for enhanced treatment of rheumatoid arthritis, Carbohydr. Polym. 316 (2023) 121018.
[24] H. Jiang, Z. Xu, Hyaluronic acid-based nanoparticles to deliver drugs to the ocular posterior segment, Drug Deliv. 30 (1) (2023) 2204206.
[25] X. Zheng, X. Li, S. Meng, G. Shi, H. Li, H. Du, L. Dai, H. Yang, Cascade amplification of tumor chemodynamic therapy and starvation with re-educated TAMs via Fe-MOF based functional nanosystem, J. Nanobiotechnol. 21 (1) (2023) 127.
[26] Y. Zhang, X. Dai, S. Yuan, Y. Zou, Y. Li, X. Liu, F. Gao, Macrophage-targeted GSH-depleting nanocomplexes for synergistic chemodynamic therapy/gas therapy/immunotherapy of intracellular bacterial infection, Biomacromolecules 25 (9) (2024) 6026–6037.
[27] M. Liu, Y. Peng, Y. Nie, P. Liu, S. Hu, J. Ding, W. Zhou, Co-delivery of doxorubicin and DNAzyme using zno@polydopamine core-shell nanocomposites for chemo/gene/photothermal therapy, Acta Biomater. 110 (2020) 242–253.
[28] Y. Chen, C. Yang, J. Mao, H. Li, J. Ding, W. Zhou, Spermine modified polymeric micelles with pH-sensitive drug release for targeted and enhanced antitumor therapy, RSC Adv. 9 (20) (2019) 11026–11037.
[29] Y. Zamudio-Cuevas, K. Martínez-Flores, G.A. Martínez-Nava, D. Clavijo-Cornejo, J. Fernández-Torres, R. Sánchez-Sánchez, Rheumatoid arthritis and oxidative stress, cellular and molecular biology (Noisy-le-Grand, France), 68(6), 2022, pp. 174–184.
[30] S. Liu, Y. Zhao, M. Shen, Y. Hao, X. Wu, Y. Yao, Y. Li, Q. Yang, Hyaluronic acid targeted and pH-responsive multifunctional nanoparticles for chemo-photothermal synergistic therapy of atherosclerosis, J. Mater. Chem. B 10 (4) (2022) 562–570.
[31] E. Montanari, C. Di Meo, A. Oates, T. Coviello, P. Matricardi, Pursuing intracellular pathogens with Hyaluronan. From a 'Pro-Infection' Polymer to a Biomaterial for 'Trojan Horse' systems, Molecules 23 (4) (2018).
[32] Z. Wang, J. Yang, Y. Yang, X. Pu, J. Zhao, N. Zhang, Targeted and combined TPCA-1-Gold nanocage therapy for in vivo treatment of inflammatory arthritis, AAPS PharmSciTech 21 (8) (2020) 298.
[33] Y. Yang, L. Guo, Z. Wang, P. Liu, X. Liu, J. Ding, W. Zhou, Targeted silver nanoparticles for rheumatoid arthritis therapy via macrophage apoptosis and Re-polarization, Biomaterials 264 (2021) 120390.
[34] F. Díaz-González, M.V. Hernández-Hernández, Rheumatoid arthritis, Med. Clínica 161 (12) (2023) 533–542.
[35] F. Zhou, M. Li, M. Chen, M. Chen, X. Chen, Z. Luo, K. Cai, Y. Hu, Redox homeostasis strategy for inflammatory macrophage reprogramming in rheumatoid arthritis based on Ceria oxide nanozyme-complexed biopolymeric micelles, ACS Nano 17 (5) (2023) 4358–4372.
[36] T. Zhu, W. Zhang, S.J. Feng, H.P. Yu, Emodin suppresses LPS-induced inflammation in RAW264.7 cells through a PPARγ-dependent pathway, Int. Immunopharmacol. 34 (2016) 16–24.
[37] L. Cheng, X. Rong, Emodin promotes the recovery of rheumatoid arthritis by regulating the crosstalk between macrophage subsets and synovial fibroblast subsets, Animal Model. Exper. Med. (2024).
[38] A. Paoletti, B. Ly, C. Cailleau, F. Gao, M.P. de Ponfilly-Sotier, J. Pascaud, E. Rivière, L. Yang, L. Nwosu, A. Elmesmari, F. Reynaud, M. Hita, D. Paterson, J. Reboud, F. Fay, G. Nocturne, N. Tsapis, I.B. McInnes, M. Kurowska-Stolarska, E. Fattal, X. Mariette, Liposomal AntagomiR-155-5p restores anti-inflammatory macrophages and improves arthritis in preclinical models of rheumatoid arthritis, Arthritis Rheumatol. 76 (1) (2024) 18–31.
[39] B. Lu, C. Li, L. Jing, F. Zhuang, H. Xiang, Y. Chen, B. Huang, Rosmarinic acid nanomedicine for rheumatoid arthritis therapy: targeted RONS scavenging and macrophage repolarization, J. Contr. Release 362 (2023) 631–646.
[40] C. Chen, Z. Lin, W. Liu, Q. Hu, J. Wang, X. Zhuang, S. Guan, X. Wu, T. Hu, S. Quan, X. Jin, J. Shen, Emodin accelerates diabetic wound healing by promoting anti-inflammatory macrophage polarization, Eur. J. Pharmacol. 936 (2022) 175329.
[41] F. Yu, N. Yu, J. Peng, Y. Zhao, L. Zhang, X. Wang, X. Xu, J. Zhou, F. Wang, Emodin inhibits lipid accumulation and inflammation in adipose tissue of high-fat diet-fed mice by inducing M2 polarization of adipose tissue macrophages, FASEB J. 35 (7) (2021) e21730.
[42] W.B. Wang, J.T. Li, Y. Hui, J. Shi, X.Y. Wang, S.G. Yan, Combination of pseudoephedrine and emodin ameliorates LPS-induced acute lung injury by regulating macrophage M1/M2 polarization through the VIP/cAMP/PKA pathway, Chin. Med. 17 (1) (2022) 19.
[43] L.P. Luo, P. Suo, L.L. Ren, H.J. Liu, Y. Zhang, Y.Y. Zhao, Shenkang injection and its three anthraquinones ameliorates renal fibrosis by simultaneous targeting IκB/NF-κB and Keap1/Nrf2 signaling pathways, Front. Pharmacol. 12 (2021) 800522.
[44] S. Cai, Y. Sun, Y. Wang, Z. Lin, Exploring the effect of LncRNA DANCR to regulate the Keap1-Nrf2/ARE pathway on oxidative stress in rheumatoid arthritis, Immu. Inflammat. Dis. 12 (1) (2024) e1163.
[45] G. Kaur, A. Sharma, A. Bhatnagar, Role of oxidative stress in pathophysiology of rheumatoid arthritis: insights into NRF2-KEAP1 signalling, Autoimmunity 54 (7) (2021) 385–397.
[46] Y. Liu, Y. Zhang, K. Zhang, Y. Wang, Protocatechuic acid reduces H(2)O(2)-induced migration and oxidative stress of fibroblast-like synoviocytes in rheumatoid arthritis by activating Nrf2-Keap1 signaling pathway, Chin. J. Physiol. 66 (1) (2023) 28–35.
[47] E.R. Puppala, S. Jain, P. Saha, M. Rachamalla, S. Np, S.S. Yalamarthi, M. Abubakar, A. Chaudhary, D. Chamundeswari, M. Usn, J.K. Gangasani, V.G.M. Naidu, Perillyl alcohol attenuates rheumatoid arthritis via regulating TLR4/NF-κB and Keap1/Nrf2 signaling pathways: a comprehensive study onin-vitro and in-vivo experimental models, Phytomedicine: Int. J. Phytotherap. Phytopharmacol. 97 (2022) 153926.
[48] A. Zhang, T. Suzuki, S. Adachi, E. Yoshida, S. Sakaguchi, M. Yamamoto, Nrf2 activation improves experimental rheumatoid arthritis, Free Radic. Biol. Med. 207 (2023) 279–295.
[49] F. Chi, C. Cheng, K. Liu, T. Sun, M. Zhang, Y. Hou, G. Bai, Baicalein disrupts the KEAP1-NRF2 interaction to alleviate oxidative stress injury by inhibiting M1 macrophage polarization, Free Radic. Biol. Med. 227 (2024) 557–569.
[50] X. Dong, J. Fu, X. Yin, S. Cao, X. Li, L. Lin, J. Ni, Emodin: a review of its pharmacology, toxicity and pharmacokinetics, Phytother Res. : PTR 30 (8) (2016) 1207–1218.